POLITECNICO
MILANO 1863

SCUOLA DI INGEGNERIA INDUSTRIALE
E DELL'INFORMAZIONE

Homework report

Guided project 1: Managing atrial fibrillation taking advantage of pseudo-electrogram measurements

Scientific computing tools for advanced mathematical modelling

Authors: Simone Piazza, Federica Valentini, Eugenio Varetti

Academic year: 2022-2023

---

1. Mathematical formulation of the problem

1.1. Checkpoint 1: classification of the atrial fibrillation mechanism

The goal of the first part of the project is to develop an algorithm to identify and classify the mechanism of atrial fibrillation by acquiring 20 endocavitary signals that describe the local activity of the heart's internal tissues.
It is possible to distinguish two types of mechanisms that generate arrhythmias:

- **Focal activity**: it is characterized by a cell generating the event, which then propagates the signal radially with respect to the point of activation.
  From the ECG, the point of activation can be identified by studying the morphology of the signal generated at that point.
- **Reentrant activity**: it occurs when an electrical signal circulates repeatedly within a closed loop in the atria, leading to multiple electrical impulses being sent out and causing the chaotic and irregular heartbeat of atrial fibrillation.

It broke down the main problem into several subproblems, namely:

1. Annotation of beats on the 20 given signals following careful pre-processing of the data to reduce noise in the signals;
2. Classification of the annotated beats into the two `QS/RS` [1] groups;
3. Classification of the overall activity into *Focal*/*Reentry* and *Both* in case there was no clear evidence in favor of either of the above.

1.2. Checkpoint 2: estimation of unknown parameters

The second checkpoint is about infering unknown parameters that characterize the applied current of the monodomain model. Depending on the mechanism (focal or reentrant), the unknown parameters would be:

- the position (x_0, y_0) of the center of the focal activity;
- the timing and length of the impulse generating a reentrant activity.

Given the signals on the 20 sensors, we can generate new signals by using a numerical approximation based on the monodomain model coupled with the Mitchell-Schaeffer model.
Then, the objective function to minimize is composed by an L^2 norm relative error and an *ad hoc* norm based on the error in activation timings:

[1] QS and RS refer to two different types of complexes that can be observed in electrocardiogram (ECG) signals. QS complexes have a negative deflection, while RS complexes have a low amplitude and a small or absent R wave.

$$\bar{\mu} = argmin \sum_{i=1}^{20} \left[\frac{||u_i - \tilde{u_i}||_2}{||u_i||_2(1 + k||\Delta T_i||_1)} + k'||\Delta T_i||_1 \right] \tag{1}$$

where:

- i is the sensor index (from 1 to 20);
- u_i is the *i-th* original signal;
- $\tilde{u_i}$ is the *i-th* signal generated by the numerical model with $\bar{\mu}$;
- k and k' are two *data-driven* coefficients;
- $||\Delta T_i||_1$ is the L^1 norm of the differences in the activation times between the given signals and the generated ones.

1.3. Checkpoint 3: reconstruction of the transmembrane potential

The goal of the last part of the project is then to reconstruct the spatial distribution of the transmembrane potential on an 11×11 grid. The action potential is a quick change in voltage across each excitable cardiac cell and it is caused by the movement of ions between inside and outside of the cells, through specific proteins called ion channels. In cardiac cells, the action potential is characterized by 5 phases:

1. Resting: the potential is stable at $\approx -90mV$ in normal working myocardial cells;
2. Upstroke: it is the phase of rapid depolarization. The membrane potential shifts into positive voltage range ($\approx 24mV$);
3. Early repolarization: this phase sets the potential for the next phase of the action potential;
4. Plateau: it is the longest phase and it marks the phase of calcium entry into the cell. It protects the cell from being depolarized again;
5. Final repolarization: it restores the membrane potential to its resting value.

Its dynamics can be reconstructed by means of the monodomain model coupled with the Mitchell-Schaeffer model. The monodomain model is a partial differential equation that enables the characterization of the propagation of the electrical impulse in the cardiac tissue; it is usually coupled with an ionic model that is solved on each degree of freedom of the computational space discretization, which in this case is the Mitchell-Schaeffer model.
The mathematical problem reads: find $u = u(x,t)$, $x \in \Omega$, $t \in (0,T]$:

$$\begin{cases} \frac{\partial u}{\partial t} = div(D\nabla u) + I_{ion}(u) + I_{app} \\ I_{ion} = J_{in} + J_{out} \\ \frac{\partial w}{\partial t} = g(w,u) \end{cases} . \tag{2}$$

where:

$$\begin{aligned} J_{in} &= \frac{wu^2(1-u)}{\tau_{in}} \\ J_{out} &= -\frac{u}{\tau_{out}} \\ g(w,u) &= \begin{cases} \frac{1-w}{\tau_{open}}, & \text{if } u < u_{gate} \\ \frac{-w}{\tau_{close}}, & \text{if } u > u_{gate} \end{cases} \end{aligned} \tag{3}$$

and D, τ_{in}, τ_{out}, τ_{open}, τ_{close}, u_{gate} are physical parameters.

2. Methods

2.1. Checkpoint 1

Annotations of beats Since the input data may contain noise generated in the measurement and/or preprocessing, it was decided to smooth them by applying moving average techniques. In particular, for the first checkpoint, the *new* data were obtained by averaging on the 10 discrete time instants around the given point. Doing so promotes proper identification of the true beat and subsequently the assignment of scores using PCA. The downside of this approach is the loss of data at the edge of the time domain (early/late beats could then be lost).
To address this issue, the following mathematical constructs were introduced to aid in the accurate identification of trigger points and beats.
A *trigger point* (or beat timing) is defined as the point of maximum negative slope of the signal, i.e., where the

first derivative has a local minimum.
For the first checkpoint, we define a *beat* as the set obtained from the trigger point and the neighbourhood of the preceding and following 30 time instants (ms).
An *early beat* is defined as a beat with an activation time of less than $30ms$; similarly, a beat with activation time within the last $30ms$ of the signal is defined as *late beat*.
For the correct identification of all early/late beats the missing part of the signal had to be reconstructed. We chose to set the latter to 0 (improvable, it could be reconstructed with regularity).

`Remark`: Since beats are identified using the local minimums search criterion, we had to include a tolerance on both the value of the minimum derivative and the period of the beat, specifically we used a *data-driven* tolerance and the period given by the average dominant cycle length.

Classification of the single beat In order to perform local classification of each annotation (QS/RS), a representative training set (Figure 1) was chosen for the two cases. Afterwards, a Principal Component Analysis (PCA) was carried out on the dataset in order to identify the bases of decomposition and obtain the scores for each observation. Given X the dataset consisting of single heartbeats over time, the mathematical problem is as follow:

1. Standardization of data:
$$Z_{ij} = \frac{X_{ij} - \bar{X_j}}{s_j}$$
where Z_{ij} is the standardized value of the (i, j)-th element of matrix X, $\bar{X_j}$ is the mean of variable j in dataset X, and s_j is the standard deviation of variable j in dataset X.
2. Computation of the covariance matrix:
$$C = \frac{1}{n-1} \sum_{i=1}^{n} (Z_i - \bar{Z})^T (Z_i - \bar{Z})$$
where C is the $p \times p$ covariance matrix, Z_i is the p-dimensional vector containing the standardized observations of the i-th row of matrix X, and $\bar{Z}$ is the p-dimensional vector containing the means of the standardized variables.
3. Calculation of eigenvalues and eigenvectors:
$$Cv_i = \lambda_i v_i$$
where v_i is the i-th eigenvector of the $p \times p$ covariance matrix C, λ_i is the i-th eigenvalue associated with the eigenvector v_i, and the index i ranges from 1 to p.
4. Selection of principal components:
Order the eigenvectors in decreasing order according to their associated eigenvalues. The first k eigenvectors that account for most of the variance in the data can be chosen as the principal components.
5. Projection of data onto the new coordinate system:
Multiply the standardized data matrix by the matrix of selected eigenvectors to obtain a new dataset of dimension $n \times k$, where k is the number of principal components selected. Here, the rows of this new dataset correspond to individual heartbeats and the columns correspond to the principal components.

It was observed that the two groups could be separated by a hyperplane. As 90% of the data variability could be explained through the first two principal components (Figure 2), a Support Vector Machine (SVM) was used to identify the best separation plane between the two groups (Figure 3).
The resulting plane was used to predict the morphology of the beats.

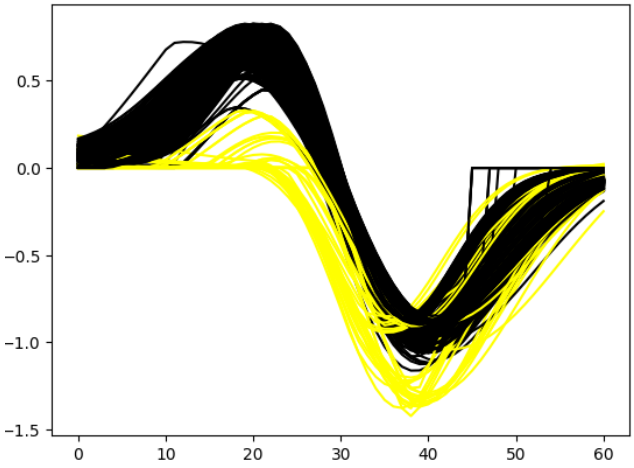

Figure 1: Training set: RS in black, QS in yellow.

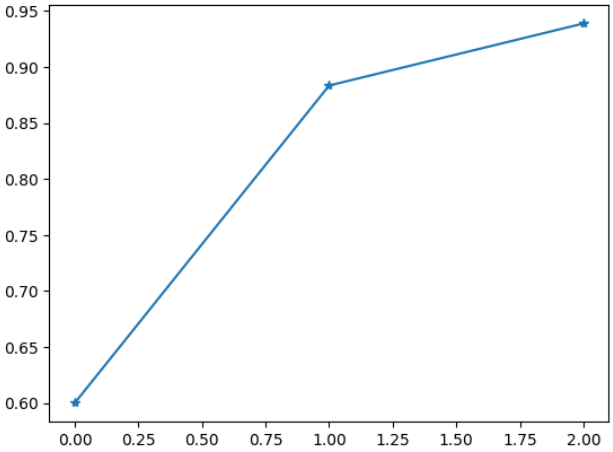

Figure 2: Cumulative variance.

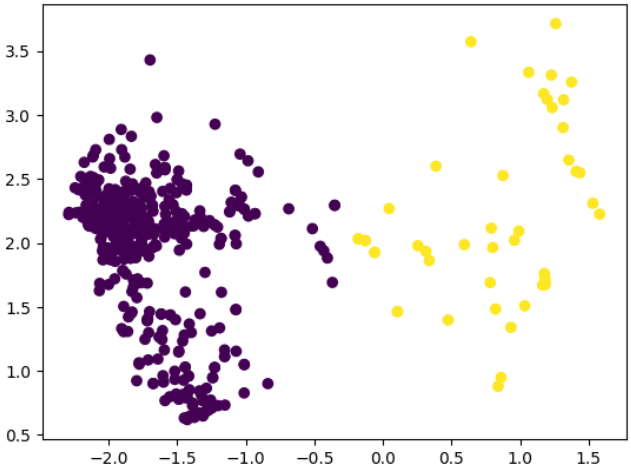

Figure 3: Scores of the PCA.

Classification of the event Once local timings and scores for each annotation are obtained, the global classification of the event is performed. Priority is given to cases where there is clear evidence of one of the two cases, in which case they will be classified accordingly. In particular, an event is defined as *focal* if there is at least one sensor where more than 50% of the recorded annotations have QS morphology.

Identification of *reentrant* activity is a bit more complicated. The algorithm can identify cases where this is *not* present with certainty. In particular, by ordering the activation times on the 20 sensors, it is possible to determine whether there is a difference between two consecutive beats greater than a portion of the Dominant Cycle Length (DCL) - chosen to be 40% as known in theory. If this exists, then reentrant activity will be excluded.
In mathematical terms, let

$$T = \{t_{11}, t_{12}, ..., t_{1n_1}, t_{21}, ..., t_{2n_2}, ..., t_{20n_{20}}\}$$

the set of all the annotations, with t_{ij} the timing of the j-th beat on the i-th sensor. Now, let $\hat{T}$ the ordered set obtained by sorting T in ascending manner. Hence, we can construct

$$\Delta = \{\delta_i\}_{i=1}^{N-1}$$

where $\delta_i = \hat{t}_{i+1} - \hat{t}_i$, with $\hat{t}_i, \hat{t}_{i+1} \in \hat{T}$, and N is the total number of annotations for the event. We define an event *reentrant* if it is not focal and if

$$\nexists \delta \in \Delta \text{ s.t. } \delta > 0.4 * DCL$$

In summary, the classification follows the following rule:.

- Focal: there exists a sensor such that more than 50% of its annotations have QS morphology (strongest hypothesis in classification);
- Reentry: if the event is not focal and if it does not exist $\delta > 0.4$*DCL;
- Both: if the event is neither focal nor reentry. Other special cases are included in this last classification but they are not reported.

2.2. Checkpoint 2

First rough estimate Since the goal of the second checkpoint is to minimize an objective function, we firstly implemented a random search algorithm. However, we wanted to exploit the physics behind the phenomena, so we stressed the data until we found out that two particular regression maps based only on timings could give us a lot more information:

Focal For each sensor i we built a map $z_i = z_i(x, y)$, $(x, y) \in \Omega$, that returns the activation times on the sensor i for a focal activity originated in (x, y) (Figure 4). Then for each sensor i we compare the real activation times with those given by the map: we add a score of 1 to all the grid nodes that generate a first activation time within a certain neighborhood of the activation time given by the *i-th* regression map.

Output: every grid node has a score from 0 to 20: the node with the greatest score is most likely to be the center of the focal activity (Figure 6).

Reentrant The procedure is similar to the one followed for the focal case: the difference consists in the fact that we were not able to build a map that could localize both the parameters at the same time. So we proceeded sequentially:

1. estimation of the Trigger **Time**: once the first activation time t with a focal morphology is found out, the Trigger time is set to $t - 2$;
2. estimation of the Trigger **Length**: we constructed several parametric maps $f_T(\delta)$, depending on the parameter T (Trigger Time). These take in input the difference in time δ between the activation times on sensor 0 and sensor 16 and return as output the Trigger Length (Figure 5).

Output: an initial guess for the two parameters is given.

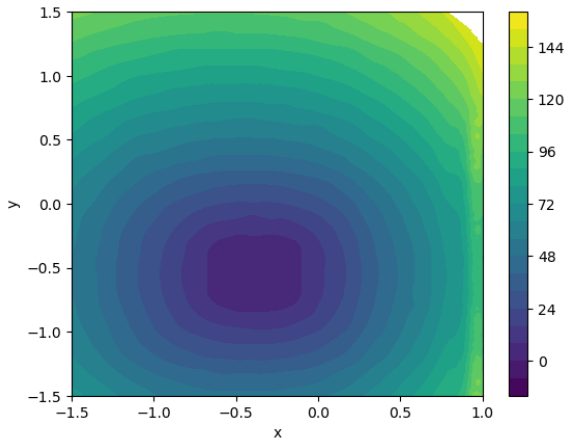

Figure 4: Example of a regression map for the focal case (sensor 15).

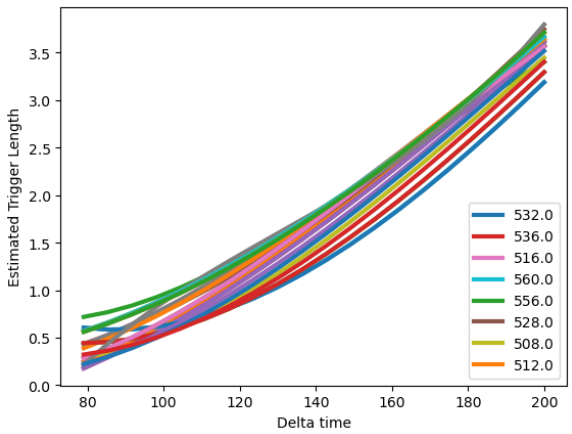

Figure 5: Parametric regression splines.

Cost function evaluation Once that a first estimate of the parameters is found, new signals are generated by imposing the parameters in a *ad hoc* neighborhood of the estimate: the goal is to find the ones that minimize the cost function. To speed up the evaluation of the functional, the code was implemented in parallel: this permits to evaluate simultaneously the functional with 8-12 (depending to the number of available cores) combination of parameters.

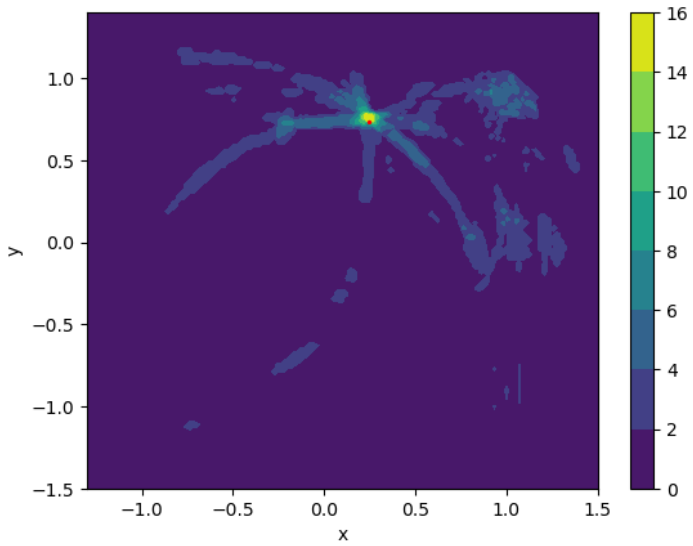

Figure 6: Score for each grid point.
The red point is the true focal position.

2.3. Checkpoint 3

Compressed sensing technique For the development of the last task of the project, i.e. the reconstruction of the spatial distribution of the transmembrane potential on an 11×11 grid, we adopted a strategy based on compressed sensing.
Mathematically, compressed sensing exploits the sparsity of a signal in a generic basis to achieve full signal reconstruction from surprisingly few measurements. Let $u \in \mathbb{R}^N$, with N "large", be the state and let $\Psi \in \mathbb{R}^{N \times N}$ be the transformation matrix; the state can be expressed as:

$$u = \Psi s \tag{4}$$

where $s \in \mathbb{R}^N$ needs to be sparse. If u admits a compressed representation with k non-zero elements in s, then the measurements $y \in \mathbb{R}^p$, with $k < p << N$, are given by:

$$y = Cu \tag{5}$$

where $C \in \mathbb{R}^{p \times n}$ is the measure matrix, which represents a set of p linear measurements on the state u and whose choice is of critical importance in compressed sensing.
The problem consists in finding the sparsest $\hat{s}$ such that:

$$y = C\Psi\hat{s} \tag{6}$$

Mathematically, this results into the resolution of the following optimization problem:

$$\begin{aligned} \hat{s} &= argmin|s|_0 \\ s.t. \quad & y = C\Psi\hat{s} \end{aligned} \tag{7}$$

where $|s|_0$ is given by the number of non-zero entries of s (i.e. its cardinality).
The main issue related to this problem is that it is a non-convex optimization problem, thus it is hard to solve. For this reason, under certain conditions on the matrix C, it is possible to reformulate (7) as:

$$\begin{aligned} \hat{s} &= argmin\|s\|_1 \\ s.t. \quad & y = C\Psi\hat{s} \end{aligned} \tag{8}$$

where $\|s\|_1$ is the ℓ_1 norm of s, given by $\|s\|_1 = \sum_k |s_k|$.
The conditions that must be verified for the ℓ_1 minimization problem (8) to converge with high probability to the sparsest solution in (7) can be summarized as:

1. The measurement matrix C must be incoherent with respect to the transformation matrix Ψ, meaning that the rows of C must not correlate with the columns of Ψ;

2. The number of measurements p must be sufficiently large, on the order of $p \simeq \mathcal{O}(k \log(N/k))$.

Transmembrane potential reconstruction In our practical application, a preliminary step must be performed before applying the compressed sensing technique: it consists, for each of the 20 sensors of the catheter, in the reconstruction of the transmembrane potential starting from the signals given as input. This objective is practically achieved through the following steps:

- Find the activation times on each sensor;
- Identify some "standard potential waves" and, for each of them, precompute the time instant in which its derivative reaches the maximum value;
- Reconstruct the action potential on each of the 20 sensors by fitting the most suitable standard-wave in such a way that, for each beat, the activation time of the signal and the time of maximum derivative of the wave coincide.

The reconstructed potential on the sensors can now be given as input to the compressed sensing algorithm, which will allow us to reconstruct the transmembrane potential on the whole 11×11 grid. Since this type of grid excludes some sensors of the catheter, we apply the compressed sensing technique to a larger grid (13×13) and at the end of the procedure we exclude its external crown in order to restore the required size of the grid to be given as output.

Construction of matrices C and Ψ The first step to perform consists in the construction of the measurement matrix C: after having defined a map from the sensors' indexes to the sensors' coordinates, the matrix C maps the space 13×13 into the sensors; in other words, it is a 20×169 matrix which has a 1 for each row i, in correspondence of the coordinate of the *i-th* sensor.
For the construction of the transformation matrix Ψ, instead, we define two different matrices depending on the global score of the event given as input; both in the focal and in the reentrant case, the matrix is constructed stacking vertically the potentials coming from a specifically built library.
After having loaded these precomputed matrices, the compressed senging minimization problem can be solved at each time step using the CVXPY library.

3. Numerical results

3.1. Checkpoint 1

Given an input signal, let us observe the macroscopic effects of the algorithm:

The input signal is given to the Python function (Figure 7).

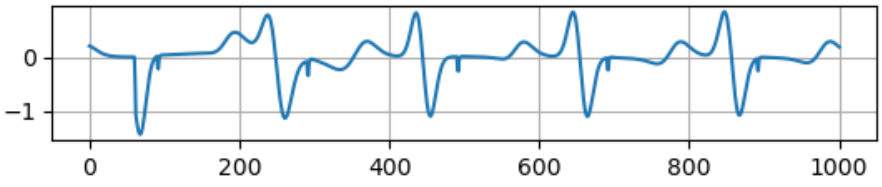

Figure 7: Input signal on one specific sensor of a spline.

The input signal undergoes smoothing, and beat annotations are obtained through a combination of derivative analysis and appropriate controls on beat frequency (Figure 8).

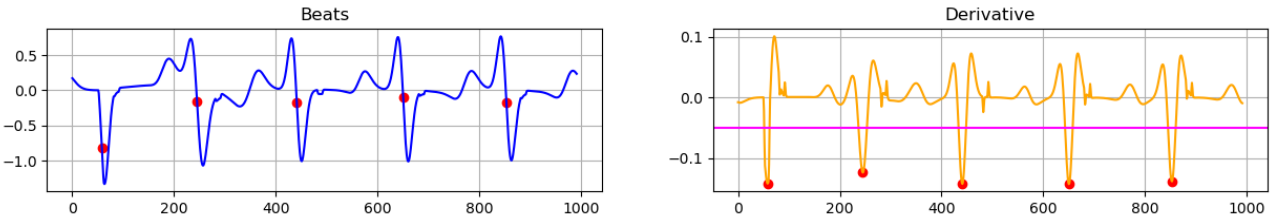

Figure 8: Smoothed signal and its derivative.

The beats are analyzed separately and classified into QS/RS (Figure 9).

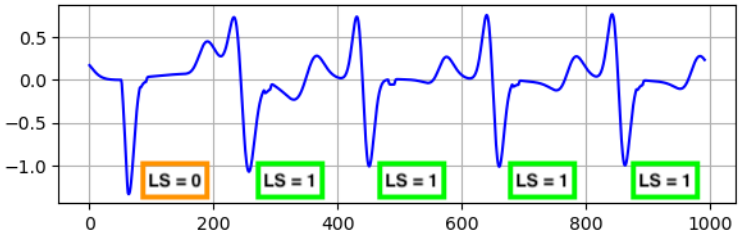

Figure 9: Every beat is classified depending on its local score: QS morphology if LS = 0, RS morphology if LS = 1.

Using the algorithm at 2.1, the test set is classified as follows:

Signal event	Type of activity
0	Reentrant
1	Focal
2	Both
3	Reentrant
4	Focal

3.2. Checkpoint 2

In the following table some numerical results are presented for the first estimate of the parameters from which the parallel search begins.

Activity Type	μ_1		μ_2	
	True	Estimate	True	Estimate
Focal	0.7500	0.75609	0.2500	0.2439
	-1.3500	-1.3414	0.2400	0.2682
	0.4000	0.3902	-0.7300	-0.7317
	-0.1100	-0.1219	0.3300	0.3170
Reentrant	510	512	1.1400	1.1648
	550	549	1.1200	1.1485
	517	518	1.1300	1.1083
	530	528	2.5000	2.594

It may be noticed how this first estimate is indeed very close to the real parameters value, in particular in the focal case; for this reason, we decided to rely only on this first estimate for the focal case, while we kept the parallel search in the reentrant case.

3.3. Checkpoint 3

Regarding the last part of the project, that is the reconstruction of the transmembrane potential on an 11×11 grid, the preliminary task consisted in the reconstruction of the potential, given the signal, on the 20 sensors of the catheter. Following the strategy specified above, the result is sufficiently accurate for our application, as can be seen in Figure 10 where the input signal is depicted in blue, the exact potential is in green and the reconstructed one is in orange.

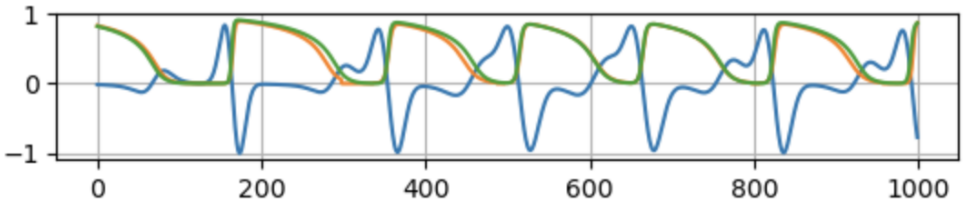

Figure 10: Reconstructed potential.

Once the potential has been reconstructed, its value every $10ms$ is used as measurement y in the compressed sensing technique: it gives as output the potential on an 11×11 grid in a small computational time (less than 2 minutes) but with a considerably large mean reconstruction error (35%), obtained computing the Frobenius norm of the error matrix. In Figure 11 is reported the output of the compressed senging algorithm at one time step for a reentrant signal: on the left there is the exact potential, in the center the potential reconstructed through compressed senging technique and on the right the error matrix given by the difference of the previous two.

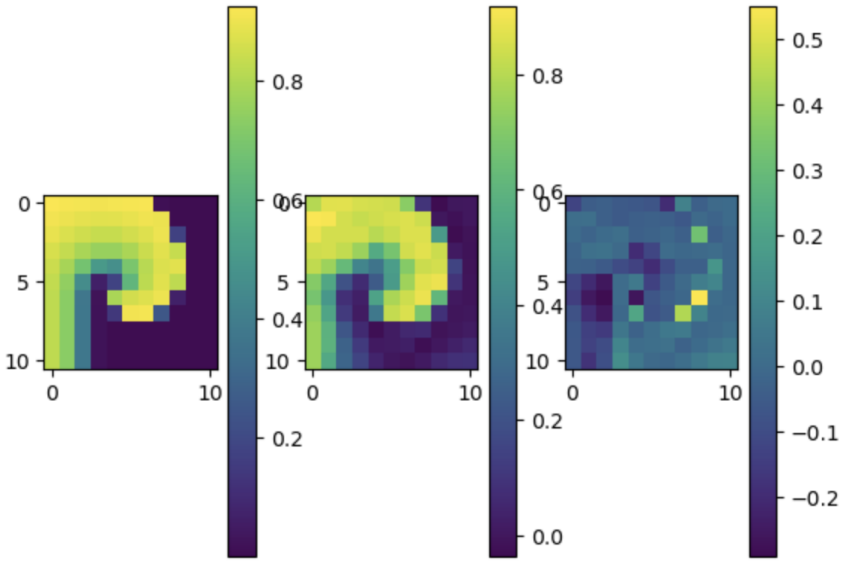

Figure 11: Output of the compressed sensing algorithm for a reentrant signal.

In order to obtain a better reconstruction of the action potential, we developed an alternative strategy that, given the input signal, takes advantage of the previously implemented algorithm to infer the unknown parameters of the signal, which are then given as input to a specific solver that computes the corresponding potential. Even if we increased the time step of the solver from $\Delta t = 0.01ms$ to $\Delta t = 0.05ms$, the computational effort required by this strategy is much larger than the previous one (approximately 15 minutes); however, we observe a significant gain in precision, indeed the error in this case is of the order of 4%. This improvement can be seen also from Figure 12, where the potential of the same signal and at the same time instant as above is reconstructed, but using this alternative approach.

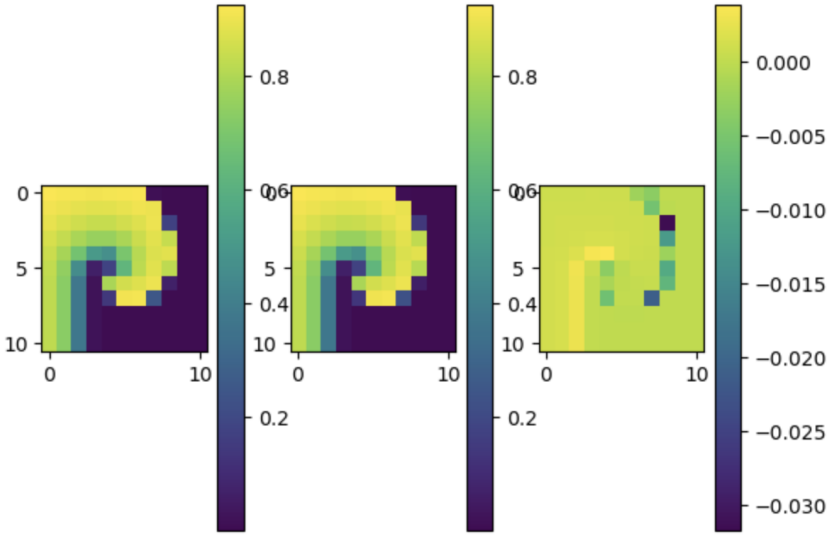

Figure 12: Reconstructed potential of the same reentrant signal but using a more precise but computationally expensive strategy.

4. Conclusions

4.1. Checkpoint 1

After analyzing the results, we can conclude that the algorithm for beat detection is effective and efficient. However, we have identified a weakness in the smoothing process that may result in the loss of very early/late beats. Although we consider this issue of secondary importance, it should be noted.
To address the issue of early/late beats, we have implemented a reconstruction method that approximates the missing part of the beat to zero. While this technique can mask the true behavior of the wave in the domain, we have found it to be a viable solution.
To improve the accuracy of the QS/RS classification, we suggest reconstructing the missing part of the wave by following the average wave behavior.
The classification algorithm was initially trained on a representative subset of waves from the test set. To further enhance the classification accuracy, we propose increasing the training set by generating precise waves with the model presented in Checkpoint 2.
Finally, the application of PCA to the training set demonstrates that the two groups (QS/RS) are linearly separable. Therefore, we suggest using an SVM to find the best hyperplane.

4.2. Checkpoint 2

Focal The procedure for the first estimate of the parameters is very consistent, especially in the inner region: the smoothness of the regression map based on the activation times allows to exploit all the information of the signals. The initial goal for this step was only to narrow the search space of the parameters, but the procedure turned out to be so effective that the search step became unnecessary.

Reentrant The procedure for the first estimate of the parameters is less effective than the one for the focal case: for this reason, we decided to keep the search in a neighborhood and to choose accordingly the evaluation of the prescribed functional.

A possible drawback of this procedure appears when the true parameters of the signal lie at the boundary of the considered domain. The regression function becomes less smooth near the boundary, thus reducing the estimation effectiveness.

4.3. Checkpoint 3

We performed the reconstruction of the transmembrane potential following two different strategies.
The compressed sensing technique has the advantage of being very efficient, but it has some limitations in terms of accuracy. Indeed, even though our libraries both for the focal and the reentrant signals are wide, the reconstruction presents some discrepancies from the exact potential, mainly in the early and late parts of the

considered time interval. The source of error could be twofold: the input of the optimization problem to be solved in the compressed sensing approach is the potential that we have previously reconstructed on the sensors of the catheter, which is though an approximation of the real one with some inaccuracies especially for small times, where the beats are often not well-defined; moreover, also the compressed sensing technique in itself represents a source of error, since it reconstructs the potential using the information available in the respective library, which is wide but surely does not include all the possible configurations of the potential at each time step.
About the second approach that we followed in order to reconstruct the potential on the grid, it is, as it was pointed out before, more precise but also more computationally expensive than the compressed sensing strategy. Its application is thus preferable only in those cases where a high accuracy is required, and a large computational time does not represent a big issue.

References

1) Cardiac Ion Channels, Augustus O. Grant (https://doi.org/10.1161/CIRCEP.108.789081)
2) https://webhome.phy.duke.edu/ qelectron/pubs/BullMathBio65_767.pdf
3) Brunton, S. L., Kutz, J. N. (2022). Data-driven science and engineering: Machine learning, dynamical systems, and control. Cambridge University Press.